Journal of Solid State Chemistry **156,** 143–153 (2001)
doi:10.1006/jssc.2000.8974, available online at http://www.idealibrary.com on IDEAL®

Excess Oxygen in Low Sr Doping $La_{1-x}Sr_xMnO_{3+\delta}$ Epitaxial Films

Keikichi Nakamura,*[,1] Mingxiang Xu,† M. Kläser,‡ and G. Linker‡

*Japan Science and Technology Corporation, Honcho 4-1-8, Kawaguchi-shi 332-0012, Japan; †Department of Physics, Zhejiang University, Hangzhou 310027, P. R. China; and ‡Forschungszentrium Karlsruhe, Institut für Festkörperforschungs, D-76021 Karlsruhe, Germany

Received May 23, 2000; in revised form August 29, 2000; accepted October 3, 2000; published online December 21, 2000

Thin films of $La_{1-x}Sr_xMnO_{3+\delta}$ ($x = 0.05$, 0.10, 0.14) on $LaAlO_3$ substrate have been prepared by employing spin coating methods. The as-prepared films crystallized at 1223 K in 1 atm oxygen show a complete in-plane epitaxy and exhibit single-crystal-like transport properties without intergrain spin-polarized scattering. In order to reduce excess oxygen, the as-prepared films were further heat-treated in 1–20 Pa oxygen at 873 to 1073 K. The excess oxygen content δ in the films was evaluated by assuming linear dependence of entropy and enthalpy of defect formation against Sr content x in the Roosmalen's defect model. The measured lattice parameters on these oxygen-reduced films show good agreement with the δ values from the above defect model. Both the calculated and the experimental results show that Mn^{4+} proportion for the as-prepared films is almost independent of Sr doping level x, and in order to get films without excess oxygen, the films must be treated in 1 Pa oxygen at 1073 K. The magnetic and transport properties measured on these films show higher T_c than the published electric phase diagram from the single crystal samples. We assumed that the La site vacancy intrinsically incorporated in the single-crystal samples during the growth process might be the cause of this difference.

Key Words: **lanthanum manganese oxide; thin film; colossal magnetoresistance; defect model; excess oxygen; Sr doping.**

1. INTRODUCTION

Oxygen nonstoichiometry of Lanthanum manganese oxide and La site substituted oxides are well known. These materials prepared in air or oxidative atmosphere contain excess oxygen. In order to get stoichiometric oxygen it is necessary to reduce oxygen under inert gas atmosphere or lower oxygen partial pressure. As for the excess oxygen δ and oxygen partial pressure relation, however, different research groups have presented different results. For example, Andersen *et al.* (1) have shown that $La_{1-x}Sr_xMnO_{3+\delta}$ ($x = 0$ to 0.3) calcined in air at 1373 K contains a Mn^{4+} proportion almost independent of Sr doping, ranging from 28% for $x = 0$ (corresponds to $\delta = 0.14$) to 31% for $x = 0.3$. This 28% Mn^{4+} in $LaMnO_{3+\delta}$ corresponds to $\delta = 0.14$. On the other hand, Toepfer *et al.* (2) have shown that in order to obtain $\delta = 0.14$ sample, it is necessary to fire the sample at 1073 K for 48 h from the sample of initial firing at 1273 K. They have also shown that the initial firing condition is very important to get higher δ value; i.e., lower firing temperature is necessary to get higher δ value sample (2). These results suggest that kinetic problems (grain size, grain shape, surface morphology, etc.) overcome thermodynamic equilibrium in this case.

As for thin films, it is not possible to apply either redox titrations or (thermo) gravimetric methods because of less than microgram-order sample weight. In previous papers (3, 4), we have shown that oxygen nonstoichiometry in $YBa_2CuO_{7-\delta}$ (YBCO) thin films can be successfully controlled by equilibrating the films simultaneously with bulk samples in a same reaction vessel. In the present case, however, it seems to be difficult to apply this method because kinetics of oxygen uptake reaction seem to be extremely slow compared with that of YBCO and depend on the initial firing temperature of bulk samples (2). Recently, Roosmalen *et al.* (5–7) have presented a defect model to describe the relation between oxygen partial pressure and excess oxygen δ. The model fits very well with the thermogravimetric data of several authors and has guided our work to determine excess oxygen in thin films.

In this report, we employed the defect model by Roosmalen *et al.* (5–7) to control and determine excess oxygen δ in $La_{1-x}Sr_xMnO_{3+\delta}$ ($x = 0.05$, 0.1, and 0.14) epitaxial films on $LaAlO_3$ substrate. After getting the desired oxygen δ value, we measured lattice constants of the films to confirm the obtained δ value. The results show that the defect model reasonably describes the pressure-δ-temperature isotherm (P-δ-T) relation and can be successfully applied to control and determine excess oxygen in thin LSMO films.

[1] To whom correspondence should be addressed at Graduate School of Integrated Science, Yokohama City University, 22-2 Seto, Kanazawa-ku, Yokohama 236, Japan. Fax: +81-45-787-2316. E-mail: keinaka@d9.dion.ne.jp.

0022-4596/01 $35.00

Another purpose of this report is to reexamine the $La_{1-x}Sr_xMnO_{3+\delta}$ electronic phase diagram from single crystal specimens (8). According to the La_2O_3–Mn_2O_3 phase diagram (9), $LaMnO_{3+\delta}$ compound has a wide range of solid solubility in both the Mn- and La-rich sides up to high temperatures, and the terminal composition in both sides are $La_{0.91}MnO_{3+\delta}$ and $La_{1.12}MnO_{3+\delta}$, respectively. Although the solid solubility decreases with increasing Sr doping level, the single-crystal samples from traveling floating zone (TFZ) methods should have a terminal nonstoichiometric composition with an appreciable amount of La vacancies. We have compared Tc values of the epitaxial thin films of $La_{1-x}Sr_xMnO_{3+\delta}$ with $x = 0$ to 0.5 with the electric phase diagram determined from the single crystal samples and have found that the agreement with that for the high Sr doping level ($x > 0.2$) is fairly good. However, with decreasing x, the data from the epitaxial films deviate from those for the single-crystal samples. We consider that the deviation comes from the intrinsic thermodynamic nature of this material. Here we present our results on $La_{1-x}Sr_xMnO_{3+\delta}$ thin films and examine these problems.

2. THE EXPERIMENTAL PROCEDURE

Stock solutions of $La_{1-x}Sr_xMnO_{3+\delta}$ ($x = 0.05$, 0.10, 0.14) were prepared from commercially available toluene-diluted naphthanates of La, Sr, and Mn in appropriate molar ratios (10, 11). In order to obtain accurate La to Mn ratio, the deviation from the initial concentration of naphthanates was corrected by measuring the weight of oxide of each component obtained by thermal decomposition. Spin coating was carried out using a laboratory constructed spin coater with a rotating speed of 2000 rpm on (100)$LaAlO_3$ (LAO). The spin-coated samples were subjected to thermal decomposition at 773 K for 10 min in air. After cooling, similar procedures were repeated until a desired thickness was obtained. In the present case we repeated this procedure two times. After the second thermal decomposition was carried out at 773 K in air, the temperature of the furnace was increased to 1223 K with a rate of 7.2 K/min, and was kept for 1.5 h. in a flowing oxygen atmosphere and then furnace cooled. During this cooling process, the temperature was kept 30 min in 973 K to equilibrate oxygen at this temperature. The films thus treated are denoted as as-prepared films. To see the effects of heat treatment under different oxygen potential, the as-prepared films were put into a quartz reaction vessel equipped with a capacitance absolute manometer (3) and annealed in a 20–1 Pa oxygen partial pressure at 873 to 1073 K. Due to the rapid kinetics of oxygen incorporation in thin films, however, we assume that the films have oxygen content equilibrated with the oxygen potentials during annealing, 10^5 and 20 to 1 Pa.

In order to get well-resolved Rutherford backscattering (RBS) yields without overlapped, strong backscattering from $LaAlO_3$ substrate, $La_{1-x}Sr_xMnO_{3+\delta}$ films were spin-coated on MgO substrates, and annealed at 973 K for 20 min. The annealing time and temperature were so determined as to avoid Mn–Mg interdiffusion (11). RBS measurements were carried out on these samples with 2 MeV He^{2+} irradiation, and the composition was determined from the scattering yield of each element divided by each cross section.

The electrical resistance and magnetoresistance (MR) were measured under 0 and 1.5 T applied field employing a four-probe method. The magnetization vs temperature curves were made using a Quantum Design MPMS SQUID magnetometer in 0.01 and 1.5 T with field parallel to the film plane.

3. OXYGEN PARTIAL PRESSURE VS EXCESS OXYGEN δ FROM THE DEFECT MODEL

In order to determine oxygen excess content δ in bulk $La_{1-x}Sr_xMnO_{3+\delta}$, two different methods have been applied. One method is to estimate δ from Mn^{4+} concentration derived from redox titrations, and another is to determine δ directly by applying *ex situ* or *in situ* gravimetric methods. For thin films, however, it is not possible to apply either gravimetric methods or redox titrations because of < 1 μg sample weights. Ar or nitrogen treatment is not suitable for the present purpose, because impurity gas level (O_2, H_2O, etc.) in such commercially available inert gas is not always the same. In the present study, we estimate equilibrium oxygen partial pressure vs excess oxygen δ by applying the defect model of Roosmalen *et al.* (5–7). This model describes the relation between oxygen equilibrium pressure P_{O_2} and excess oxygen δ, Sr doping concentration x, and the degree of disproportionation of Mn^{3+} into Mn^{4+} and Mn^{2+}, ξ. The parameter ξ also expresses the upper limit of excess oxygen δ defined as $\delta < \xi/2$. The defect model leads to Eq. [1]

$$K_v = (P_{O_2})^{-3/2} \frac{(1 - x - 2\xi + 2\delta)^6 3^3 \delta^2}{(\xi - 2\delta)(3 + \delta)^2} = (P_{O_2})^{-3/2} f(\delta), \quad [1]$$

where K_v is the equilibrium constant for defect formation and its temperature dependence can be expressed as

$$-RT \ln K_v = \Delta H_v - T\Delta S_v$$

$$= \frac{3}{2}(\Delta \bar{H}_{O_2} - T\Delta \bar{S}_{O_2}) - RT \ln f(\delta) \quad [2]$$

or

$$\ln Kv = -\frac{\Delta H_v}{RT} + \frac{\Delta S_v}{R} \quad [3]$$

and

$$\Delta H_v = \frac{3}{2}\Delta\bar{H}_{O_2} \quad [4]$$

$$\Delta S_v = \frac{3}{2}\Delta\bar{S}_{O_2} + R\ln f(\delta), \quad [5]$$

where ΔH_v and ΔS_v are enthalpy and entropy of defect formation, and $\Delta\bar{H}_{O_2}$ and $\Delta\bar{S}_{O_2}$ are the relative partial molar quantities which can be obtained from the temperature dependence of oxygen partial pressure P_{O_2} at a given δ. Thus if the relative partial molar quantities for excess oxygen are known (these quantities are usually obtained at higher temperature as 1200–1400 K), $P - \delta - T$ relation at lower temperatures (873–973 K) can be obtained using Eqs. [1]–[5], provided that these quantities do not depend significantly on temperature.

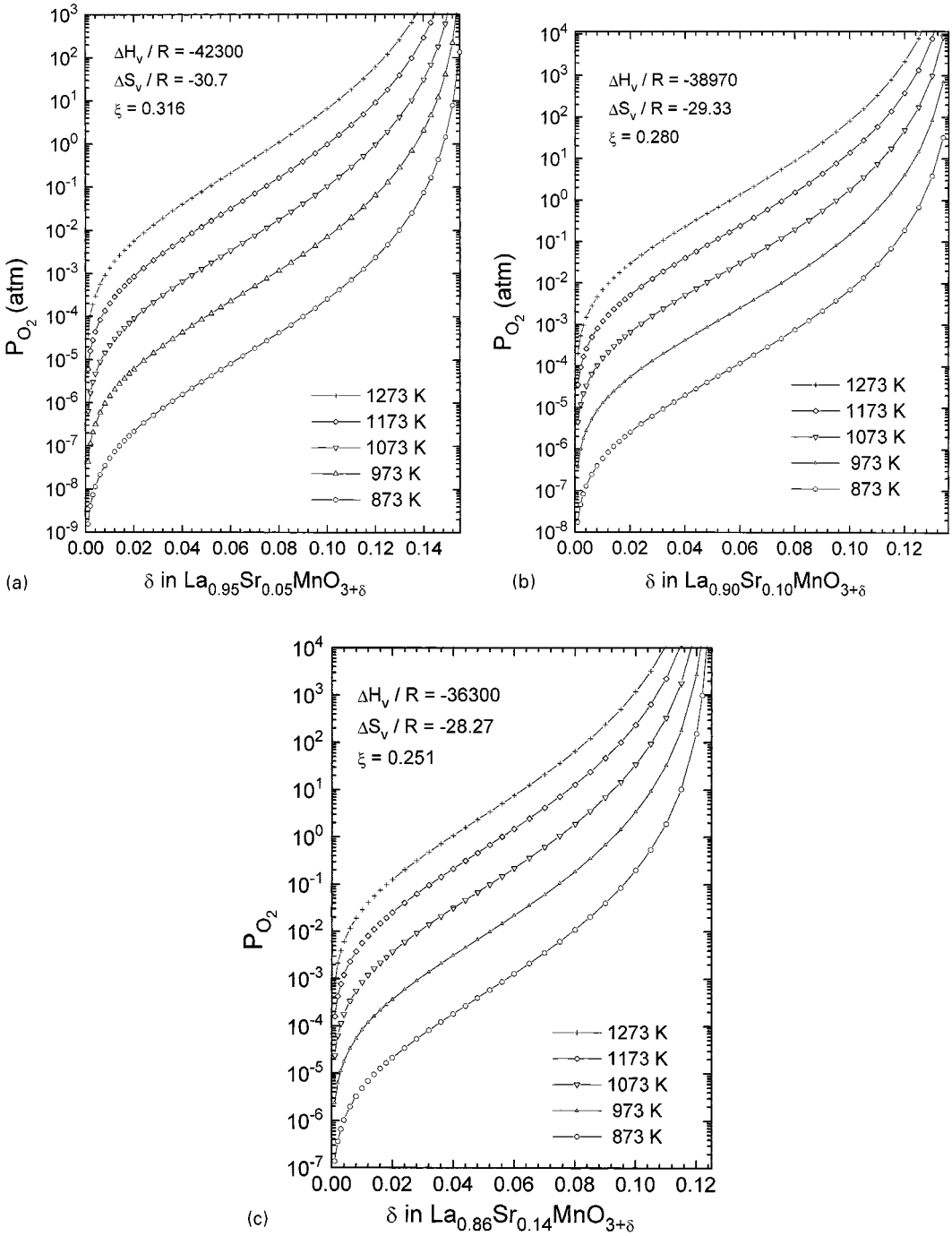

FIG. 1. Calculated isotherms for equilibrium oxygen partial pressure vs excess oxygen δ in $La_{1-x}Sr_xMnO_{3+\delta}$ films for (a) $x = 0.05$, (b) $x = 0.10$, and (c) $x = 0.14$.

For $La_{1-x}Sr_xMnO_{3+\delta}$, Kuo *et al.* (12) have presented partial molar quantities for $x = 0$, 0.01, 0.05, 0.1, and 0.2. Their $\Delta\bar{H}_{O_2}$ values were almost independent of x, ranging from -114.5 to -115.8 KJ/mol O_2. The values are, however, too small compared with those for $LaMnO_3$, -253.4 KJ/mol O_2 (7), -230 KJ/mol O_2 (13), and -197 KJ/mol O_2 (7) for $La_{0.85}Sr_{0.15}MnO_{3+\delta}$. Thus, it would produce large errors if values from Kuo *et al.* are applied to calculate lower temperature (873 to 973 K) $P-\delta-T$ relation. Because of this reason, we employed Roosmalen's quantities (ΔH_v, ΔS_v, ξ) for $x = 0$ and 0.15 and calculated those for $x = 0.05$ to 0.14 by assuming that there are linear relations between x and these quantities. We believe that this assumption is reasonable. For example, the measured partial molar entropies at a fixed δ value by Kuo *et al.* show also a linear relation with x. Further evidence is that the upper limit of δ values (corresponding to $\xi/2$ in Eqs. [1]–[5] decreases with x, $\delta = 0.18$ for $x = 0$ (calcined at 1073 K, Ref. (2)) to almost zero for $x = 0.3$ when calcined in air at 1373 K (1). Using $\Delta H_v/R = -45700$, $\Delta S_v/R = -32.0$, and $\xi = 0.352$ for $x = 0$ and $\Delta H_v/R = -35600$, $\Delta S_v/R = -28.0$, and $\xi = 0.244$ for $x = 0.15$, we have estimated those for $x = 0.05$, 0.10, and 0.14 assuming linear relations with respect to x. The calculated values are $\Delta H_v/R = -42300$, $\Delta S_v/R = -30.7$, and $\xi = 0.316$ for $x = 0.05$, and $\Delta H_v/R = -38970$, $\Delta S_v/R = -29.33$, and $\xi = 0.280$ for $x = 0.10$, and $\Delta H_v/R = -36300$, $\Delta S_v/R = -28.30$, and $\xi = 0.251$ for x = 0.14, respectively. $P-\delta-T$ relations for $x = 0.05$, 0.10, and 0.14 from 873 to 1273 K calculated using these parameters are shown in Figs. 1a to 1c.

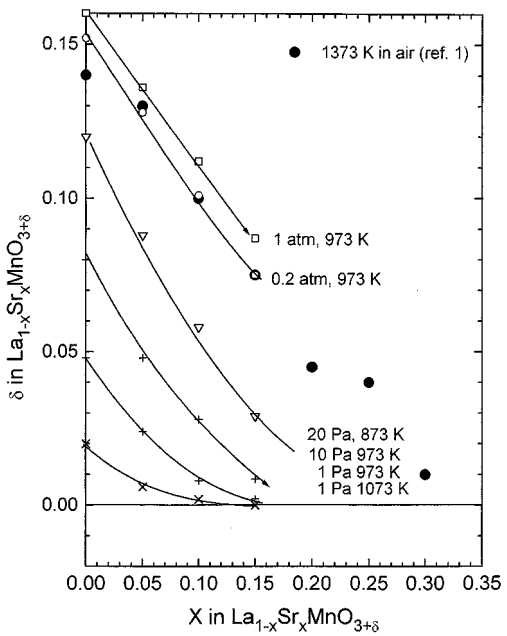

FIG. 2. Plots of equilibrium δ values against Sr doping x for $La_{1-x}Sr_xMnO_{3+\delta}$ annealed at 873 to 1073 K in 1 to 10^5 Pa oxygen partial pressures.

Figure 2 shows plots of calculated equilibrium δ at three different temperatures, 873, 973, and 1073 K, and oxygen partial pressures, 10^5, 20–1 Pa. In order to compare the calculated values with the experimental values, calculated values for $x = 0.15$ instead of 0.14 are plotted here. Experimental δ values annealed in air (1) are also shown in the same figure. The calculated δ values in 1 atm oxygen show a linear decrease with x, which is consistent with experimental results of Andersen *et al.* (1), except that the temperature exhibiting almost the same δ value is about 400 K higher in the experimental values than in the calculation. One of the possible reasons for this is that the polycrystalline $La_{1-x}Sr_xMnO_{3+\delta}$ samples, after being equilibrated at 1373 K, may incorporate additional oxygen during the cooling process.

At higher temperatures and lower equilibrium pressures, the δ vs x plots show asymptotic behavior with respect to the $\delta = 0$ line. This asymptotic behavior suggests that films with different x can be treated under the same conditions to get almost zero δ values. For example, the equilibrium δ values at 1073 K in 1 Pa O_2 are 0.0012, 0.0018, and 0.06 for $x = 0.15$, 0.10, and 0.05, respectively.

4. Mn^{4+} PROPORTION IN $La_{1-x}Sr_xMnO_{3+\delta}$ EPITAXIAL FILMS

So far most colossal magnetoresistance (CMR) thin films were obtained under sufficient oxygen partial pressure or

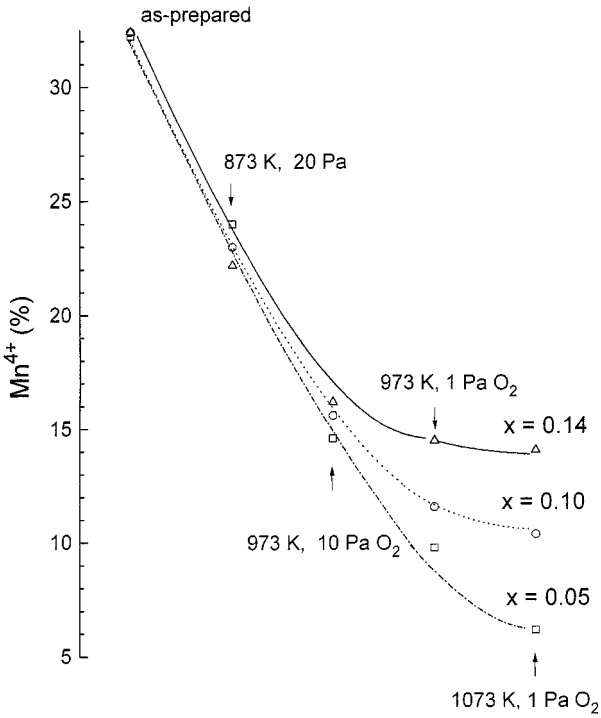

FIG. 3. Change in Mn^{4+} proportion in $La_{1-x}Sr_xMnO_{3+\delta}$ with different annealing temperature and oxygen partial pressure.

were heat-treated under oxidative atmosphere (mostly 1 atm O_2). Under such conditions, most thin films contain enough oxygen corresponding to equilibrium at an ambient temperature if films were quenched rapidly to room temperature. Under such annealing and cooling conditions, thin films and bulk powder have the same oxygen potential, and the excess oxygen content in thin films can be, in principle, obtained by applying either redox or gravimetric methods. In the present, however, oxygen uptake and reduction kinetics of thin film and bulk $LaMnO_3$ materials are not well established. Because of this reason, it seems to be difficult to employ simultaneous annealing in a constant oxygen partial pressure which was used to equilibrate YBCO thin films and the bulk (3, 4). In this report, we annealed as-prepared films in constant oxygen partial pressure and quickly cooled the films to room temperature by taking off the quartz reaction vessel from the furnace.

Important and interesting information from Eqs. [1]–[5] and Fig. 1 is the change in Mn^{4+} proportion with annealing temperatures and pressure. Figure 3 shows the change in Mn^{4+} concentration with different oxygen reduction conditions, 873 to 1073 K and 20 to 1 Pa. It is astonishing that the Mn^{4+} proportion is independent of Sr doping for annealing conditions 973 K in 1 atm, 873 K 20 Pa, and at 973 K in 10 Pa O_2. From the figure one can also see that oxygen reduction at 1073 K in 1 Pa O_2 is enough to obtain samples without excess oxygen. The maximum Mn^{4+} proportion (32%) for the as-prepared films (annealing 973 K in 1 atm O_2) is in accordance with the experimental values (1, 2). The calculated results in Fig. 3, together with the experimental facts, suggest that oxygen reduction treatments are very important for obtaining films with M_n^{4+} content consistent with La site dopings.

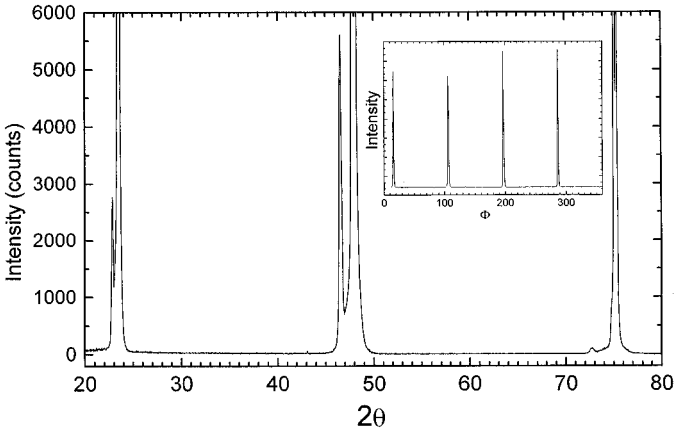

FIG. 5. X-ray diffraction patterns of as-prepared $La_{0.9}Sr_{0.1}MnO_{3+\delta}$ films. (Inset) Φ Scan for the same film.

5. RESULTS

Figure 4 shows RBS yields of thin films with nominal composition x (determined by weighting the naphthanate solution) 0.05, 0.10, and 0.14, respectively. In order to avoid overlap of backscattering yield from each element, the thickness of the films was thinner than the films on $LaAlO_3$

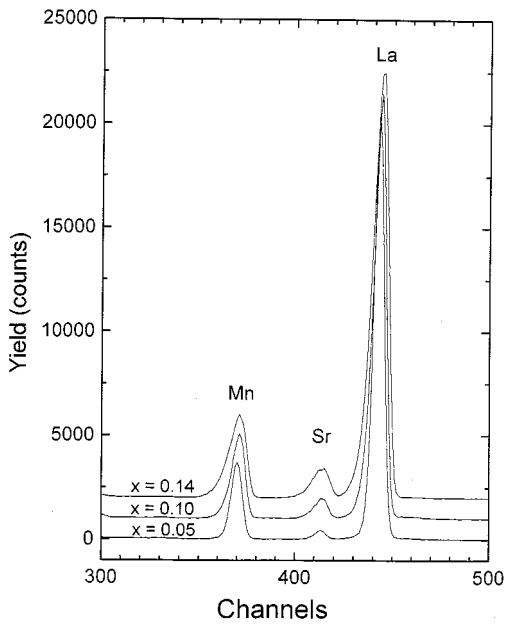

FIG. 4. RBS yields of $La_{1-x}Sr_xMnO_{3+\delta}$ films on MgO substrate for $x = 0.5$, 0.10, and 0.14.

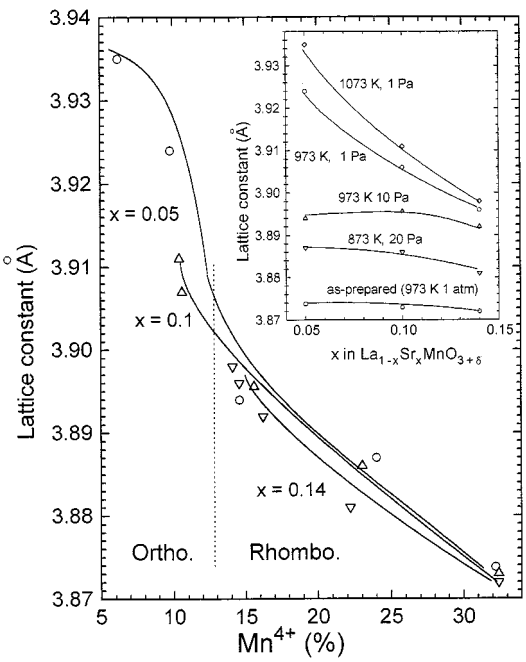

FIG. 6. Lattice constant vs Mn^{4+} proportion for $La_{1-x}Sr_xMnO_{3+\delta}$ films. (Inset) Lattice constant vs x in $La_{1-x}Sr_xMnO_{3+\delta}$ for different annealing processes.

substrate and is different for different samples. From the backscattering yields, the compositions were estimated to be $La_{0.955}Sr_{0.045}Mn_{1.02}O_{3+\delta}$, $La_{0.90}Sr_{0.10}Mn_{1.02}O_{3+\delta}$, and $La_{0.865}Sr_{0.135}Mn_{0.98}O_{3+\delta}$. The RBS results show fairly good agreement with the nominal compositions.

Figure 5 shows an X-ray diffraction θ–2θ scan for an as-prepared $La_{0.9}Sr_{0.1}MnO_{3+\delta}$ (estimated δ is 0. 095) film. The inset to the figure shows an in-plane (220, pseudocubic cell) scan for the same film. Two sharp peaks assigned to rhombohedral (012) and (024) lines ((001) and (002) of

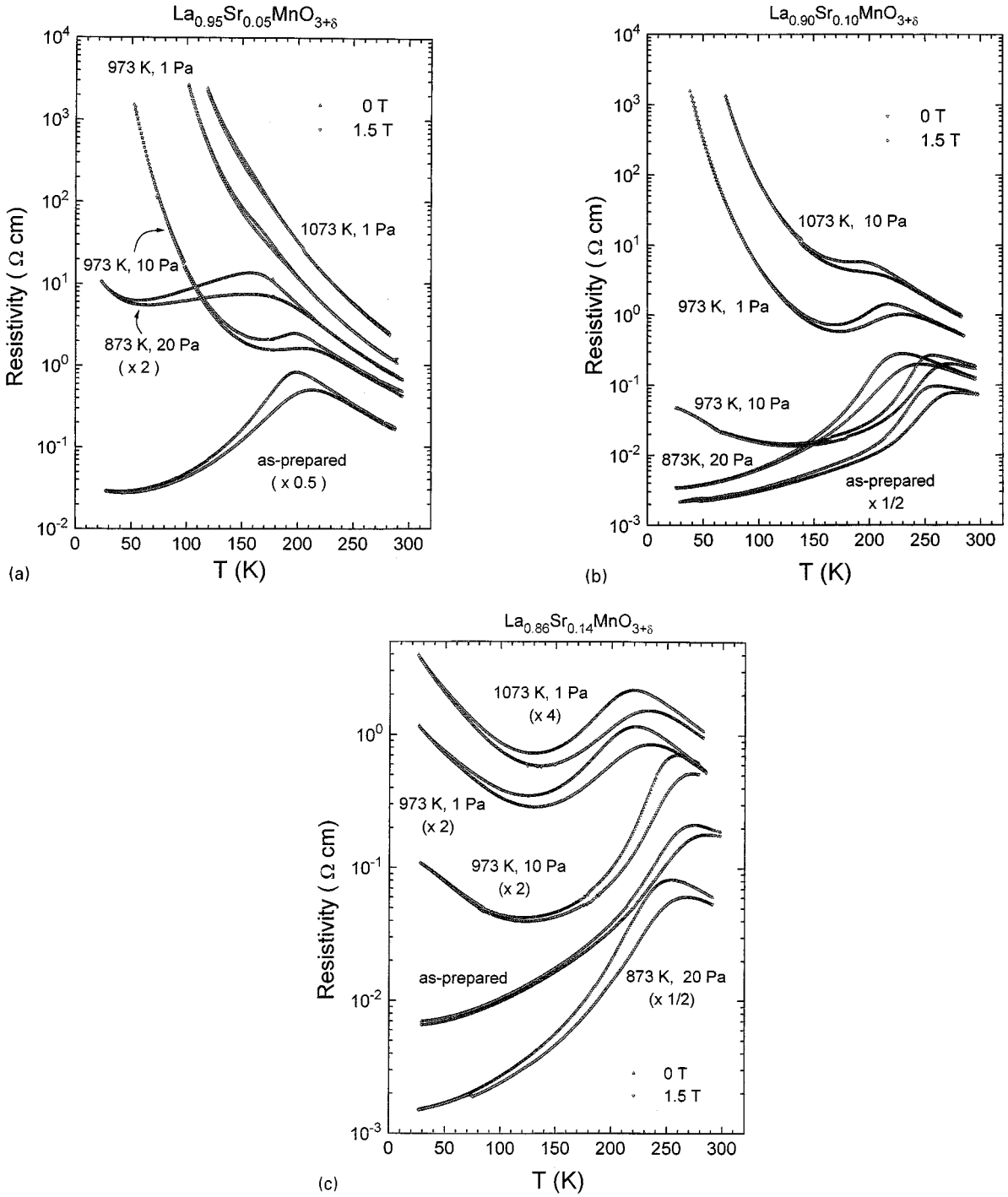

FIG. 7. Temperature dependence of the resistivity for $La_{1-x}Sr_xMnO_{3+\delta}$ films annealed at different oxygen partial pressures and temperatures: (a) $x = 0.05$, (b) $x = 0.01$, and (c) $x = 0.14$.

pseudocubic cell) can be seen at about 1–1.5° lower angle of the same rhombohedral $LaAlO_3$ strong lines. Figure 6 shows the change in lattice parameter (along the growth direction) vs Mn^{4+} proportion. The Mn^{4+} proportions were estimated from the $P-\delta-T$ relations in Figs. 1a–1c. Inset to the figure shows variation of the lattice parameter with different oxygen reduction treatments. From the inset, the lattice constant with oxygen reduction treatment under 10 Pa or more higher oxygen pressure is almost independent of Sr doping level, suggesting that Mn^{4+} proportion in these films annealed above 10 Pa O_2 should be almost equal, as shown in Fig. 3. The plots of lattice parameter against Mn^{4+} concentration in the figure show two different regions characterized by different gradients against Mn^{4+} proportion. From 30 to ca. 13 Mn^{4+} %, which can be assigned to the rhombohedral region, the lattice parameter changes 0.0013 Å/% Mn. Between ca. 13 to 5%, which can be assigned to the orthorhombic region, the lattice parameter changes abruptly and gradually decreases its gradient with decreasing Mn^{4+} proportion. In the same figure lattice parameters by Jonker (14) are also plotted. The lattice parameters of the films in the rhombohedral region are almost equal to that measured by Jonker (14). This suggests that strain from the $LaAlO_3$ substrate (lattice mismatch 2.3%) does not significantly affect the present epitaxial films, which is also consistent with the fact that the strain from the substrate becomes negligible when the film thickness is thicker than 100 nm.

Figures 7a to 7c show the temperature dependence of resistivity for $La_{1-x}Sr_xMnO_{3+\delta}$ ($x = 0.05$, 0.10, 0.14) films with different oxygen reduction treatments. Because the room temperature resistivity changes little with the reduction of oxygen compared with the significant change in the low-temperature region, the resistivity curves around room temperature overlap. To avoid such overlap, some curves are multiplied by 4 to $\frac{1}{2}$ times to shift to higher or lower sides. An examination of the figure shows that the as-prepared films (973 K in 1 atm O_2) show metallic resistivity behavior below resistivity peak maximum temperature independent of degree of Sr doping. With the reduction of excess oxygen at 873 K in 20 Pa, the resistivity peak temperature decreases and the resistivity increases but the difference from the as-prepared samples is small. Under this reduction treatment, the film with minimum Sr doping, 0.05, shows an upturn in the resistivity curve at about 50 K, but the films with $x > 0.1$ still show metallic behavior below the ferromagnetic transition temperature. For the films oxygen reduced at 973 K under 10 Pa oxygen, all the films with $x < 0.14$ show resistivity upturn below ferromagnetic transition temperature, especially for the sample with $x = 0.05$, which shows clear insulating behavior at lower temperatures.

Figures 8a, 8b, and 8c compare the temperature dependence of magnetization (10 Oe), resistivity, and MR curves. Here, MR is defined as $(\rho_H - \rho_0)/\rho_H$ ($H = 1.5$ T). The magnetization is normalized with unit area (emu/cm^2). Comparing the three curves, the resistivity peak temperature Tp is almost equal to the ferromagnetic transition temperature Tc, but the MR peak temperature is about 20 to 8 K lower than the resistivity peak Tp. The difference between the resistivity and MR peaks becomes smaller with decreasing δ or Mn^{4+} content. For $La_{0.9}Sr_{0.1}MnO_{3+\delta}$ film annealed at 973 K in 1 Pa, the difference becomes 8 K. In the present case, we have observed a MR peak at 160 K for the lowest Mn^{4+} concentration of 6% of $La_{0.95}Sr_{0.05}MnO_{3.006}$ (1073 K, 10 Pa), where no resistivity peak can be observed, as shown in Fig. 7. This suggests that the magnetic transition temperature can also be estimated from the MR peak temperature. Figure 8c also shows that with decreasing excess oxygen, zero-field cooled (ZFC) and field-cooled (FC) runs show different behavior. Such behavior was observed in $LaMnO_{3+\delta}$ with $0 < \delta < 0.07$ region and was assigned to spin-glass magnetic behavior (2). The δ region where such spin-glass behavior appears is different with doping level x in Sr doped films, $\delta < 0.01$ in $x = 0.14$, $\delta < 0.02$ in $x = 0.10$ and $\delta < 0.05$ in $x = 0.05$.

Figure 9 plots resistivity peak temperature Tc of the films against Mn^{4+} proportion. Tc does not decrease monotonously with decreasing Mn^{4+} concentration. Two peaks, local minima and maxima, can be observed. The depth of the local minimum observed around Mn^{4+} 25% becomes shallower with increasing Sr doping. This suggests that T_c cannot be solely determined by Mn^{4+} proportion. Probably, Mn and La site (especially Mn site) vacancies may play another important role in determining T_c.

Figure 10 plots MR at 1.5 T against reduction of excess oxygen. From the figure, the magnetoresistance seems to behave quite differently for oxygen reduction. For higher doping level as $x = 0.14$, MR increases with decreasing excess oxygen but this trend is reversed with decreasing x value as shown in the figure.

Figure 11 plots Tc on the $La_{1-x}Sr_xMnO_3$ electronic phase measured on single-crystal samples fabricated by traveling floating zone (TFZ) methods (8). The Tc from the sol–gel-derived films is located between the two dotted lines for all δ values studied here. At higher Sr doping as $x = 0.3$, the difference between T_c of the TFZ single crystal (369 K) and that of the sol–gel film (365 K, Ref. 10) is 4 K. However, with decreasing Sr doping, the difference becomes significant. Especially, the difference around $x = 0.1$ is as large as 50 K. This difference possibly arises from the fact that the $LaMnO_3$ system has a large solid solubility both in the La and Mn rich side, and the single crystal samples from TFZ methods should contain La or Mn site vacancies corresponding to the terminal composition in equilibrium with the coexisting liquid phase.

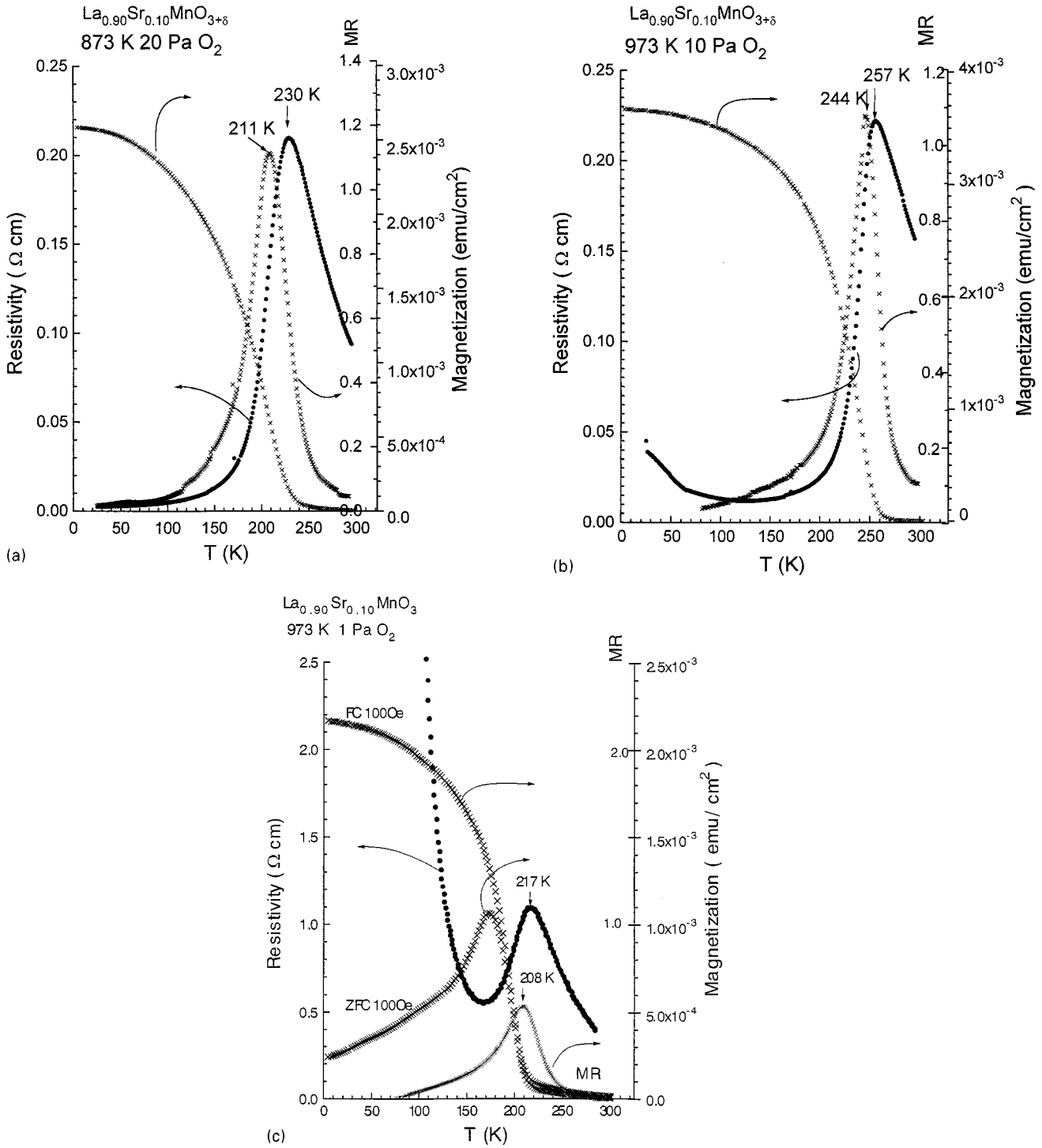

FIG. 8. Correlation between the temperature dependence of resistivity, magnetization and, magneto-resistance curves for $La_{0.9}Sr_{0.1}MnO_{3+\delta}$ thin films: (a) 873 K, 20 Pa O_2, (b) 973 K, 10 Pa O_2, and (c) 973 K, 1 Pa O_2.

6. DISCUSSION

In this study, the Mn^{4+} proportion for the as-prepared films is almost independent of Sr doping concentration. The Mn^{4+} proportion keeps Sr doping independent until the oxygen reduction treatment makes excess oxygen for the highest Sr doping sample ($x = 0.14$) close to zero (see Fig. 2, Mn^{4+} 16% at 973 K 10 Pa). These calculated results from

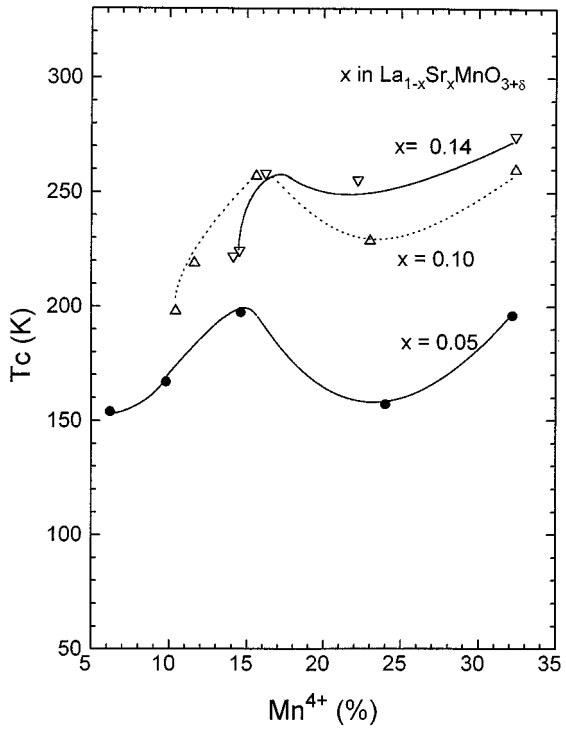

FIG. 9. Resistivity peak temperature (ferromagnetic onset temperature) vs Mn^{4+} proportions in $La_{1-x}Sr_xMnO_{3+\delta}$ films.

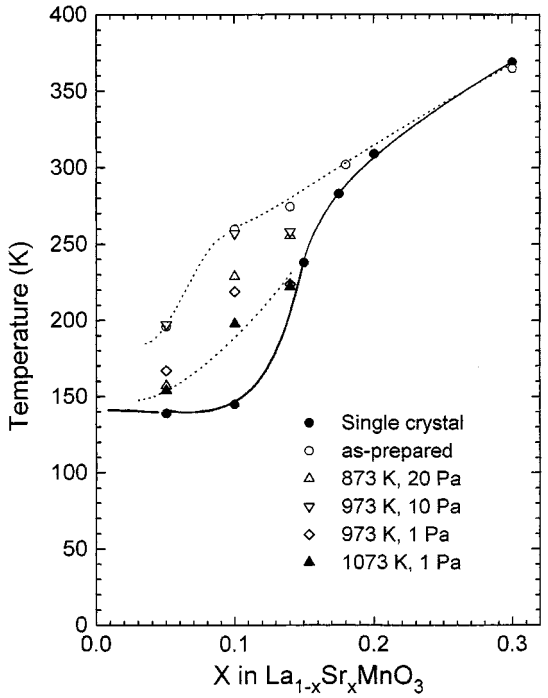

FIG. 11. Resistivity phase transition points for $La_{1-x}Sr_xMnO_{3+\delta}$ films with different oxygen reduction treatments are plotted on the electronic phase diagram for a single crystal of $La_{1-x}Sr_xMnO_{3+\delta}$.

the defect model by Roosmalen *et al.* (5–7) are consistent with the experimental results of Andersen *et al.* (1), indicating that the defect model is suitable for describing the $P-\delta-T$ relation in this system. In order to understand schematically why the Mn^{4+} proportion is independent of Sr doping concentration, the $P-\delta-T$ curves at 973 K for different x values are plotted in Fig. 12. From the figure, it is easily shown that, at higher pressures, the interval of the isotherm curves, $\Delta\delta$, for different x is just equal to the half of the difference in x, $\Delta\delta = \Delta x/2$. For example, the interval $\Delta\delta$ is 0.04/2 between $x = 0.14$ to 0.1 isotherm curves and 0.05/2 between $x = 0.10$ to 0.05 and 0.05 to 0 isotherm curves. This means that the increase in Mn^{4+} proportion generated by Sr doping is compensated by the decrease in excess oxygen δ. This relation is good down to 10^{-4} atm. For pressure less than 10^{-5} atm, where excess oxygen δ for $x = 0.15$ becomes close to zero, this relationship is no longer valid and the Mn^{4+} proportion becomes close to the value from pure Sr doping contribution, as can be seen in Fig. 3.

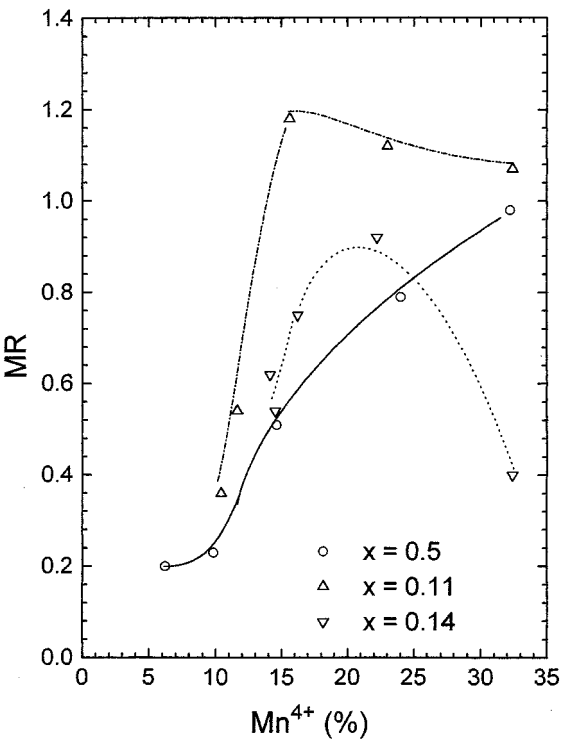

FIG. 10. Magnetoresistance ratio vs Mn^{4+} proportion for $La_{1-x}Sr_xMnO_{3+\delta}$ films.

From the $P-\delta-T$ isotherm curves, it becomes clear that in the doped $LaMnO_{3+\delta}$ system, doping of divalent cations does not change Mn^{4+} concentration if samples are prepared under 1 atm. For Sr doping less than 0.15, Mn^{4+} proportion is almost independent of Sr doping down to 20 Pa at 973 K. According to Toepfer *et al.* (2), however, the magnetic and transport properties of $LaMnO_{3.11}$ to $LaMnO_{3.14}$ (Mn^{4+} 22 to 28%) are very much different from those of $La_{0.8}Sr_{0.2}MnO_3$ to $La_{0.72}Sr_{0.28}MnO_3$, both of them have the same doping level (Mn^{4+} 22 to 28%). In this

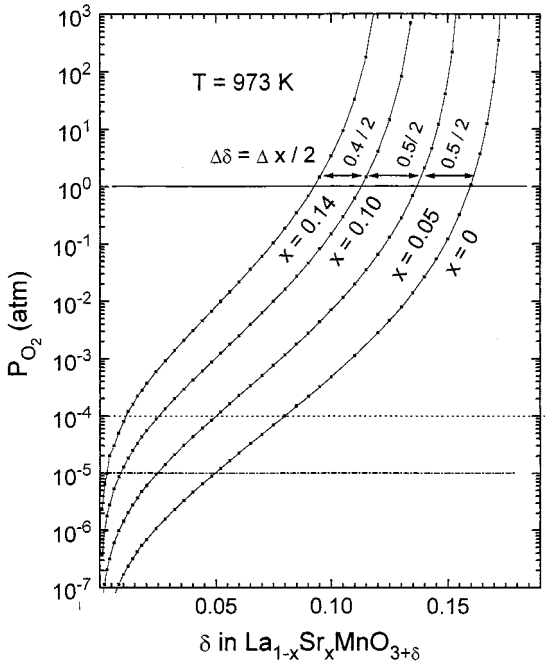

FIG. 12. Isotherms for $P-\delta-T$ relation at 973 K for different x values. The double arrows show that the interval between each isotherm curves are just equal to the change in δ necessary to compensate the increase in Mn^{4+} proportion with x. This relation is valid at higher pressures, but no more valid at lower pressures.

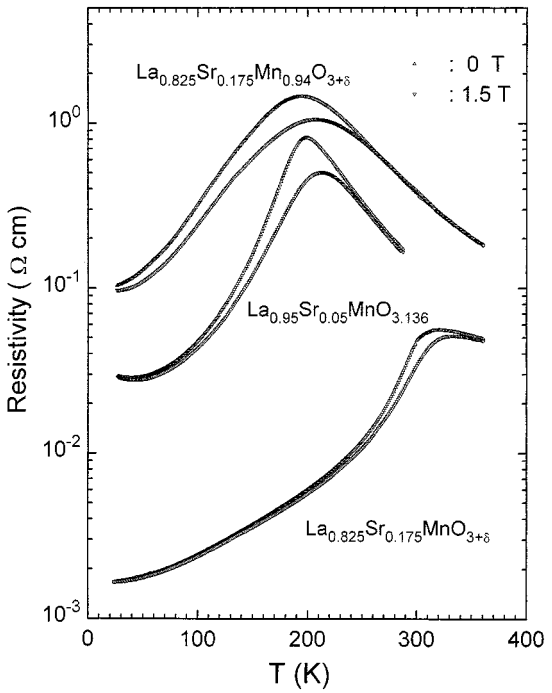

FIG. 13. Comparison of temperature dependence of resistivity curves for $La_{0.825}Sr_{0.175}MnO_{3+\delta}$, Mn site vacancy doped $La_{0.825}Sr_{0.175}Mn_{0.94}O_{3+\delta}$, and as-prepared $La_{1-x}Sr_xMnO_{3.136}$ thin films.

doping level, $LaMnO_{3+\delta}$ shows ferromagnetic insulator behavior with ferromagnetic transition temperature of 180 to 200 K, whereas $La_{1-x}Sr_xMnO_3$ shows ferromagnetic metal behavior with T_c 320 to 365 K. This means that such physical properties are not solely determined by the Mn^{4+} proportion.

Although the crystal structure, lattice parameter, and unit cell volume of doped $LaMnO_{3+\delta}$ do not depend strongly on the kind of dopant, the physical properties seem to depend strongly on the kind of dopant and occupied sites. The difference in the effects of La site substituted Sr and excess oxygen is that excess oxygen creates equal amounts of La and Mn site vacancies. For $La_{1-x}Sr_xMn_{3+\delta}$, it is better expressed as (2)

$$(La_{1-x}Sr_x)_{1-\varepsilon}Mn_{1-\varepsilon}O_3 \qquad \text{with} \quad \varepsilon = \frac{\delta}{3+\delta}. \qquad [6]$$

With decreasing Sr doping, the Mn and La site vacancy concentration increases to keep the Mn^{4+} proportion constant. Thus, for $La_{0.95}Sr_{0.05}MnO_{3.135}$ (as-prepared film, 973 K 1 atm), Mn site vacancy amounts to 4.3%. Such Mn site vacancy would affect strongly the Mn–O–Mn double exchange interaction energy in the same manner as in the case of Mn site substitution (15–17). Figure 13 shows how the Mn site vacancy affects transport properties. The films denoted $La_{0.825}Sr_{0.175}MnO_{3+\delta}$ (estimated $\delta = 0.075$, $\varepsilon = 0.025$) and $La_{0.825}Sr_{0.175}Mn_{0.94}O_{3+\delta}$ are differen in the (La + Sr)/Mn ratio. The latter film had Mn site vacancies intentionally introduced within the solid solubility range of 0.1. Due to the intentionally doped Mn site vacancy, the resistivity behavior changed significantly as shown in the figure. In the same figure, resistivity for $La_{0.95}Sr_{0.05}MnO_{3.136}$ is also plotted for comparison. The Mn site vacancy ε for this film is estimated to be 4.3%, which is smaller than the intentionally doped Mn site vacancy 6%, but the two resistivity curves have nearly the same resistivity maximum temperature. Since the La site vacancy improves resistivity behavior significantly (increase T_c and decrease resistivity) as is well known from the self-doped $La_{1-\Delta}MnO_{3+\delta}$ system (18), the Mn site vacancy might be one of the reasons for the degraded magnetic and transport properties of low Sr doping samples.

It is also interesting to compare the magnetotransport properties of the epitaxial films and those of the single crystal samples. T_c values of the as-prepared films plotted in Fig. 11 deviate from the phase diagram, since an appreciable amount of excess oxygen is incorporated into the films. The good agreement observed in the $x = 0.3$ region implies that both samples were prepared in the same oxygen partial pressure (1 atm O_2) and contain close to zero excess oxygen. At a lower Sr doping level, $x < 0.15$, the deviation becomes significant. For $x = 0.14$, the resistivity curve (Fig. 7b) for

the epitaxial film shows a resistivity peak at 224 K and shows metallic conductivity below the transition temperature, although a clear resistivity upturn is observed around 130 K. On the other hand, the resistivity curve for the single-crystal sample for $x = 0.15$ shows a clear insulating behavior below T_c. Similarly, the resistivity behavior for $x = 0.1$ film also shows different behavior from the single-crystal one. The plots of T_c on the phase diagram shown in Fig. 11 show a significant deviation between the two around $x = 0.1$.

According to Takeda *et al.* (18), the solid solubility of the La site vacancy in the Mn-rich side decreases with increasing Sr doping, i.e., 10% for $x = 0$ (i.e., $La_{0.9}MnO_{3+\delta}$), 7% for $x = 0.1$ (i.e., $(La_{0.9}Sr_{0.1})_{0.93}MnO_{3+\delta}$), and 3% for $x = 0.3$ (i.e., $(La_{0.7}Sr_{0.30})_{0.97}MnO_{3+\delta}$). It is possible that the solid solubility changes with oxygen partial pressure because La and Mn site vacancies generated by excess oxygen change with pressure, and the change in vacancy concentration might affect entropy of mixing. However, the phase diagram in air shows that the solid solubility in Mn-rich side keeps almost the same value ($La_{0.9}MnO_{3+\delta}$) independent of temperature. These results suggest that the single-crystal samples from TFZ method should have a terminal nonstoichiometric composition equilibrated with the liquid phase and should contain an appreciable amount of La vacancies. Thus for $La_{0.9}Sr_{0.1}MnO_{3+\delta}$, single crystal fabricated in air should have ca. 7% La(Sr) site vacancy corresponding to 20.3% Mn^{4+} increase. If the single-crystal sample thus fabricated has a Mn^{4+} proportion of 10%, it must have $0.203/2 \cong 0.10$ oxygen deficiency to compensate for the increase in Mn^{4+} % proportion due to La(Sr) site vacancy to give the resultant composition as $(La_{0.9}Sr_{0.1})_{0.93}MnO_{2.90}$. Both vacancies compensate the change in Mn^{4+} proportion and the resultant Mn^{4+} proportion is just equal to that for the stoichiometric composition $La_{0.9}Sr_{0.1}MnO_3$. Such oxygen site vacancies also affect the Mn–O–Mn double exchange energy and would degrade the magnetotransport properties, as has been experimentally confirmed by Guidara *et al.* (19) for oxygen-deficient $La_{0.6}Sr_{0.4}MnO_{3-\delta}$.

In summary, we have examined the defect model by Roosmalen *et al.* (5–7) and have successfully controlled and determined the level of excess oxygen for low Sr doping. The calculated $P - \delta - T$ relations assuming linear dependence of enthalpy and entropy of defect formation indicate that the Mn^{4+} proportion of as-prepared films is almost independent of Sr doping. The measured lattice parameters vs δ relation on these oxygen-reduced films also show good agreement with the calculated δ values. In order to get films without excess oxygen δ, the Sr-doped films must be treated in 1 Pa oxygen at 1073 K. The magnetic and transport properties measured on these films show higher T_c than the electric phase diagram from the single-crystal samples. The La site vacancy intrinsically incorporated in the single-crystal samples during the growth process might be the cause of this difference.

REFERENCES

1. I. G. Krogh Andersen, E. Krough Andersen, P. Norby, and E. Skou, *J. Solid State Chem.* **113,** 320 (1994).
2. J. Toepfer and J. B. Goodenough, *J. Solid State Chem.* **130,** 117 (1997).
3. K. Nakamura, J. Ye, and A. Ishii, *Physica C* **213,** 1 (1993).
4. J. Ye and K. Nakamura, *Phys. Rev. B* **48,** 7554(1993).
5. J. A. M. Roosmalen and E. H. P. Cordfunke, *J. Solid State Chem.* **110,** 106 (1995).
6. J. A. M. Roosmalen and E. H. P. Cordfunke, *J. Solid State Chem.* **110,** 109 (1995).
7. J. A. M. Roosmalen and E. H. P. Cordfunke, *J. Solid State Chem.* **110,** 113 (1995).
8. A. Urushibara, Y. Morimoto, T. Arima, A. Asamitsu, G. Kido, and Y. Tokura, *Phys. Rev B* **51,** 14103 (1955).
9. J. A. M. Roosmalen, D. van Vlaaderen, E. H. P. Cordfunke, W. L. Ljdo, and D. J. W. Ijdo, *J. Solid State Chem.* **114,** 516 (1995).
10. T. Manabe, I. Yamaguchi, W. Kondo, S. Mizuta, and T. Kumagai, *J. Mater. Res.* **12,** 541 (1997).
11. K. Nakamura, X. Liu, T. Hatano, Z. Jiao, K. Shang, and A. Ishii, *Jpn. J. Appl. Phys.* **39,** 1721 (2000).
12. J. H. Kuo and H. U. Andersen, *J. Solid State Chem.* **83,** 52 (1989).
13. N. Kamegashita, Y. Miyazaki, and H. Yamamoto, *Mater. Chem. Phys.* **11,** 187 (1984).
14. G. H. Jonker, *Physica* **22,** 707 (1956).
15. K. H. Ahn, X. W. Wu, K. Liu, and C. L. Chien, *Phys. Rev. B* **54,** 15299 (1996).
16. J. W. Cai, C. Wang, B. G. Shen, J. G. Ahao, and W. S. Zhan, *Appl. Phys. Lett.* **71,** 1727 (1997).
17. A. Anane, C. Dupas K. Le Dang, J. P. Renard, P. Veillet, L. Pinsard, and A. Revcolevschi, *Appl. Phys. Lett.* **69,** 1160 (1996).
18. Y. Takeda, S. Nakai, T. Kojima, R. Kanno, N. Imanishi, G. Q. Shen, O. Yamamoto, M. Mori, C. Asakawa, and T. Abe, *Mater. Res. Bull.* **26,** 153 (1991).
19. K. Guidara, E. Dhahri, and J. C. Joubert, *Phase Transitions* **68,** 607 (1999).